



Multi-population mortality forecasting using high-dimensional functional factor models

Chen Tang  *

Research School of Finance, Actuarial Studies and Statistics
Australian National University

Han Lin Shang 

Department of Actuarial Studies and Business Analytics
Macquarie University

Yanrong Yang 

Research School of Finance, Actuarial Studies and Statistics
Australian National University

September 10, 2021

Abstract

This paper proposes a two-fold factor model for high-dimensional functional time series (HDFTS), which enables the modeling and forecasting of multi-population mortality under the functional data framework. The proposed model first decomposes the HDFTS into functional time series with lower dimensions (common feature) and a system of basis functions specific to different cross-sections (heterogeneity). Then the lower-dimensional common functional time series are further reduced into low-dimensional scalar factor matrices. The dimensionally reduced factor matrices can reasonably convey useful information in the original HDFTS. All the temporal dynamics contained in the original HDFTS are extracted to facilitate forecasting. The proposed model can be regarded as a general case of several existing functional factor models. Through a Monte Carlo simulation, we demonstrate the performance of the proposed method in model fitting. In an empirical study of the Japanese subnational age-specific mortality rates, we show that the proposed model produces more accurate point and interval forecasts in modeling multi-population mortality than those existing functional factor models. The financial impact of the improvements in forecasts is demonstrated through comparisons in life annuity pricing practices.

Keywords: Age-specific mortality forecasting; Factor models; Functional panel data; Functional principal component analysis; Multilevel functional data.

*Postal address: Research School of Finance, Actuarial Studies and Statistics, Level 4, Building 26C, Australian National University, Kingsley Street, Acton, Canberra, ACT 2601, Australia; Email: chen.tang@anu.edu.au.

1 Introduction

The continuing improvements in human life expectancy and mortality have exposed many stakeholders of the society with longevity risk, such as governments, health care systems and life insurance industries. Hence, accurate forecasting of mortality rates is paramount. Over the past century, modeling and forecasting age-specific mortality rates have become an ongoing endeavor of many scholars. Among those, the Lee-Carter model ([Lee and Carter, 1992](#)) is one of the most remarkable developments, which is the ground that many extensions are derived from ([Renshaw and Haberman, 2003](#); [Hyndman and Ullah, 2007](#); [Giroso and King, 2008](#); [Li et al., 2013](#); [Wiśniowski et al., 2015](#)). These works focused on modeling the mortality of a single population. One of the major criticisms of forecasting single populations individually is that increasing divergence in the long-run mortality rates (see, e.g., [Pampel, 2005](#); [Li and Lee, 2005](#); [Li, 2013](#)). To overcome this, joint modeling and forecasting mortality for multiple populations has begun to gain popularity in demographic research. In addition, joint mortality models could improve forecast accuracy by exploring additional common information from other populations (see, e.g., [Shang, 2016](#)).

However, the aforementioned advantages does not come for free. New problems arise when modeling multi-population mortality rates jointly. That is, we need to work with multi-population mortality data with increasing volume and complicated structure. On one hand, increasing volume means that the multi-population mortality data consist of mortality rates of a large number of populations (cross-sections), which is the area of high-dimensional data analysis ([Cai and Chen, 2010](#); [Bühlmann and Van De Geer, 2011](#)). On the other hand, the complicated structure of the multi-population mortality data lies in how the age-specific mortality rates of each population are formed. For each population, mortality rates of all ages are recored for different years. The age-specific mortality rates at any given year can be regarded as a curve, which falls in the functional data analysis (FDA) framework (see, e.g., [Ramsay and Silverman, 2006](#); [Ferraty and Vieu, 2006](#); [Horváth and Kokoszka, 2012](#); [Kokoszka and Reimherr, 2017](#)). Moreover, the age-specific mortality rates curves are recorded sequentially according to time, hence, they form functional time series (FTS) ([Hörmann et al., 2010](#)). Therefore, modeling the multi-population mortality data is a problem lying in the intersection of high-dimensional data analysis and functional time series analysis, i.e., high-dimensional functional time series (HDFTS).

In modeling multi-population mortality data as HDFTS, there are two sources of ‘curse of dimensionality’ ([Bellman, 1966](#)). First, we have mortality data from a large number of populations;

second, the mortality rates from each population are a collections of dependent infinite dimensional curves. In high-dimensional data analysis, dimension-reduction techniques, such as principal component analysis (PCA) (see [Jolliffe and Cadima, 2016](#), for an intensive review) or factor analysis ([Gaskin and Happell, 2014](#)) are applied first. In modeling functional time series, to incorporate the temporal dependence within each curve, functional version of dynamic principal component analysis [Panaretos and Tavakoli \(2013a\)](#); [Hörmann et al. \(2015\)](#); [Rice and Shang \(2017\)](#) and functional version of factor models([Hays et al., 2012](#); [Liebl et al., 2013](#); [Jungbacker et al., 2014](#); [Kokoszka et al., 2015](#); [Martínez-Hernández et al., 2020](#)) are adopted.

However, factor models for high dimensional FTS can be found sporadically in the literature. [Di et al. \(2009\)](#) introduce the multilevel FPCA (MFPCA), which performs classic FPCA on intra- and inter-subject geometric components of multilevel functional data. [Shang \(2016\)](#) applies MFPCA to model mortality rates of multiple populations. MFPCA could be easily extended to model panels of FTS by incorporating dynamic FPCA. Because FTS in the panel could exhibit heterogeneity across different sets, [Tang et al. \(2021\)](#) propose a clustering method to obtain homogeneous sets of FTS before they can be modeled jointly. [Gao et al. \(2019\)](#) model HDFTS using a two-step approach to represent the N functional time series with several univariate time series, which relies on FPCA with the same truncation level on each FTS and many factor models. [Nisol et al. \(2019\)](#) argue that using PCA projection for each FTS before a global PCA projection does not guarantee the common component of all sets will be picked. Therefore, they set up high-dimensional functional factor models for panels of functional time series. Let N is the number of sets of FTS, and T is the number of curves in each set of FTS. Due to the computational intense of performing the eigendecomposition of $\mathbf{X}_{NT}\mathbf{X}_{NT}^\top$, [Nisol et al. \(2019\)](#) obtain the factor loading indirectly. They performs an eigendecomposition of $\mathbf{X}_{NT}^\top\mathbf{X}_{NT}$ to obtain the factors and then multiply the factors back with \mathbf{X}_{NT} . [Chang et al. \(2020\)](#) propose an auto-covariance-based learning framework for functional time series to improve estimation, but their focus is not on forecasting.

Apart from the work in modeling HDFTS listed above, [Wang et al. \(2019\)](#) propose a factor model for matrix-structured data, i.e., matrix-valued time series, as they believe that the columns and rows of a matrix represent different information that is interrelated in a structural way. So, it would be beneficial to maintain the matrix structure rather than breaking the matrix into a long vector. In their work, they use a front-loading matrix to reflect the effect along the row of the data matrix and a back-loading matrix to reflect the effects across the column of the data matrix. The

factor matrices are a low-dimensional matrix-values time series which contains all the temporal information.

Motivated by their work, we extend the front and back loading matrices to functional versions and propose a factor model for HDFTS to forecast multi-population mortality rates. In our model, we first reduce the dimensions along the populations, in which we decompose the HDFTS into FTS with lower dimensions (common feature) and a system of basis functions specific to different populations (heterogeneity). By doing this, the heterogeneity within different populations can be separated by allowing for different back-loading curves. The HDFTS can then be represented by a small panel of functional time series, representing the homogeneous feature among all populations. We then apply a functional factor model to the small panel of functional time series to obtain the front functional loading. In this way, the lower-dimensional common functional time series can be reduced into low-dimensional scalar factor matrices. The temporal information contained in the multi-population data can be extracted into these low-dimensional scalar factor matrices, which facilitates forecasting. This separation of heterogeneity and homogeneity fits perfectly in the multi-population mortality data modeling as it allows for some heterogeneous patterns existing in the mortality rates of each population and forecasts of different populations based on the homogeneous feature will not diverge in the long-run.

In addition to the adaptability to the multi-population mortality data, our proposed model enjoys additional benefits in terms of flexibility. That is, the proposed model can be viewed as a general case of several existing models [Di et al. \(2009\)](#); [Nisol et al. \(2019\)](#); [Gao et al. \(2019\)](#), by setting the front and back functional loadings to certain forms, our model can be reduced to these models.

In the empirical analysis, we compare the in sample forecasting performance of the proposed model with that of the aforementioned functional factor models and several other multi-population mortality models ([Dong et al., 2020](#)). We find that the proposed high-dimensional functional factor model produces more accurate point and interval forecasts than the other models. Furthermore, the financial impact of the improvements in the forecast is demonstrated through the life annuity pricing, the proposed model could lead to a significant save on the reserve for life insurers.

The rest of the paper is organized as follows. Section 2 details the factor model. Section 3 outlines the estimation procedures. Section 4 describes the forecasting method based on the factor model for HDFTS. Section 5 presents the simulation studies to show the finite sample performance

of model fitting and forecasting of the proposed method. Section 6 presents empirical analysis on the Japanese subnational mortality data. Section 7 concludes this paper.

2 Factor model for high-dimensional functional time series

We propose a new two-fold factor model for HDFTS, which separates the homogeneity and heterogeneity within the data. The homogeneity represents the similarity that shared all the cross-sections, while the heterogeneity represents the dissimilarity. By doing this, we reduce the dimension of the high-dimensional time series. The temporal information of the original data could be summarized into a low-dimensional matrix-valued time series. In this vein, the curse of dimensionality is addressed, and forecasts are feasible. The development and interpretation of the model are provided in detail in this section.

2.1 Data structure

Let $\{\mathcal{X}_t : t = 1, \dots, T\}$ be an N -dimensional functional time series, where N is the number of sets of functional time series, and T is the sample size or the number of functions within each set of functional time series. The HDFTS can be organized into a single matrix format, such that

$$\mathbf{X}(u) = \begin{bmatrix} \mathcal{X}_1^{(1)}(u) & \mathcal{X}_1^{(2)}(u) & \dots & \mathcal{X}_1^{(N)}(u) \\ \mathcal{X}_2^{(1)}(u) & \mathcal{X}_2^{(2)}(u) & \dots & \mathcal{X}_2^{(N)}(u) \\ \vdots & \vdots & \ddots & \vdots \\ \mathcal{X}_{T-1}^{(1)}(u) & \mathcal{X}_{T-1}^{(2)}(u) & \dots & \mathcal{X}_{T-1}^{(N)}(u) \\ \mathcal{X}_T^{(1)}(u) & \mathcal{X}_T^{(2)}(u) & \dots & \mathcal{X}_T^{(N)}(u) \end{bmatrix}$$

where $\mathbf{X}(u)$ is a $T \times N$ matrix, each entry in the matrix, $\mathcal{X}_t^{(i)}$, for $i \in 1, \dots, N$ and $t \in 1, \dots, T$ is defined in $\mathcal{H} := \mathcal{L}^2(\mathcal{I})$, a Hilbert space of square integrable functions on a real interval $\mathcal{I} \in [a, b]$, with the inner product $\langle f, g \rangle = \int_{\mathcal{I}} f(u)g(u)$ and the norm $\|\cdot\| = \langle \cdot, \cdot \rangle^{\frac{1}{2}}$.

Under our setting, the i^{th} column of $\mathbf{X}(u)$, $\mathcal{X}^{(i)}(u) = [\mathcal{X}_1^{(i)}(u), \dots, \mathcal{X}_T^{(i)}(u)]^{\top}$, where $i \in \{1, 2, \dots, N\}$, represents a set of functional time series, which contains serial dependence. Alternatively, the t^{th} row of $\mathbf{X}(u)$, $\mathcal{X}_t(u) = [\mathcal{X}_t^{(1)}(u), \dots, \mathcal{X}_t^{(N)}(u)]$, where $t \in \{1, 2, \dots, T\}$, consists of functions of all cross-sections N at a specific time t . It is noteworthy that these are correlated. Taking the age-specific mortality rate as an example, each entry in $\mathbf{X}(u)$ represent the age-specific mortality rate curve of a specific country at specific time. The i^{th} column of $\mathbf{X}(u)$ represents the

mortality rate curves of country i across the sample period, and the t^{th} row of $\mathbf{X}(u)$ represents the mortality rate curves of all countries at time t .

2.2 Model setup

Denote $\mathcal{Y}_t^{(i)}(u) = \mathcal{X}_t^{(i)}(u) - \mu^{(i)}(u)$, such that $\{\mathcal{Y}_t^{(i)}(u) : t = 1, \dots, T\}$ be the centered functional time series. Let us consider the following factor model for the centered HDFTS

$$(2.1) \quad \mathcal{Y}_t^{(i)}(u) = \phi(u)\mathbf{F}_t\boldsymbol{\lambda}^{(i)\top}(u) + \epsilon_t^{(i)}(u), \quad t = 1, 2, \dots, T,$$

where $\phi(u)$ is a vector of length r , with each entry being functional, it is the features common to all sets of functional time series; \mathbf{F}_t is an $r \times k$ matrix; $\boldsymbol{\lambda}^{(i)}(u)$ is a vector of length k , with each entry being functional, it is specific for each $i \in \{1, \dots, T\}$, which reflects the specific characteristic (heterogeneity) of each set of functional time series; and $\epsilon_t^{(i)}(u)$ is white noise idiosyncratic process that has no serial dependence (see, e.g., [Lam et al., 2011, 2012](#)). We term $\phi(u)$ and $\boldsymbol{\lambda}^{(i)}(u)$ the front factor loading and back factor loading, respectively, [Wang et al. \(2019\)](#) also use these terms for their model. The difference is that in their work the factor loadings are scalar-valued while in the proposed model the factor loadings are function-valued.

2.3 Model interpretation

The proposed model can be interpreted in the following ways. We use the back functional factor loading to characterize the heterogeneity of the functional time series cross-sections. By separating the heterogeneity, the original data is reduced into multivariate functional time series of smaller dimensions. These common multivariate functional time series characterizes the original data's homogeneity. After reducing the dimensions of these common multivariate functional time series, the temporal information is captured by low-dimensional matrix-valued time series which facilitates forecasting. The detailed interpretation is described as follows.

2.3.1 Dimension reduction along cross-sections

Denote $\mathcal{F}_t^\top(u) = \phi(u)\mathbf{F}_t$, then model in (2.1) can be expressed as

$$(2.2) \quad \mathcal{Y}_t^{(i)}(u) = \boldsymbol{\lambda}^{(i)}(u)\mathcal{F}_t(u) + \epsilon_t^{(i)}(u),$$

where $\boldsymbol{\lambda}^{(i)}(u)$ is a k -dimensional functional factor loading vector, $\boldsymbol{\lambda}^{(i)}(u) = [\lambda_1^{(i)}(u), \dots, \lambda_k^{(i)}(u)]$, with each entry being a function, defined previously, $\mathcal{F}_t(u)$ is a $k \times 1$ vector of functional factors. This model is different from [Nisol et al. \(2019\)](#), where the factor loading is functional and factors are scalar. Here, the functional factor loading $\boldsymbol{\lambda}^{(i)}(u)$ is dependent on i , which represents the heterogeneity of each set of functional time series. While the functional factor $\mathcal{F}_t(u)$ is common to all i , which represents the common features of the HDFTS. Then $\mathcal{F}(u) = [\mathcal{F}_1(u), \dots, \mathcal{F}_T(u)]^\top$ is a k -dimensional FTS ($k \ll N$). By doing this, we separate the common features of the HDFTS, $\mathcal{F}(u)$, from the heterogeneity, $\boldsymbol{\lambda}^{(i)}(u)$, and reduce the HDFTS to functional time series with smaller dimension.

[Bai \(2009\)](#) propose a panel data model with interactive fixed effects where the multiplication of the r -dimensional factor loading $\boldsymbol{\lambda}_i$ and the r -dimensional common factors \mathbf{F}_t in the factor structure can be viewed as the interaction of these two terms. The interactive effects model is more general than the additive effects model. It allows the individual effect of i and the time effect of t to be involved in the model interactively rather than additively, giving more flexibility. [Freyberger \(2018\)](#) argue that the interactive fixed effects model could handle cases where heterogeneity is not time-homogeneous. [Tang et al. \(2021\)](#) propose a functional panel data model with additive fixed effects. To handle the time-varying heterogeneity, they further propose a clustering algorithm to search for homogeneous subgroups before jointly modeling the functional time series sets. Our model can be viewed as a functional extension of the interactive fixed-effects model, as stated in (2.2), both the factor loading $\boldsymbol{\lambda}^{(i)}(u)$ and the common factors $\mathcal{F}_t(u)$ are functional, where $\boldsymbol{\lambda}^{(i)}(u)$ captures the specific effects of different cross-sections and $\mathcal{F}_t(u)$ denotes the common features, the multiplication of $\boldsymbol{\lambda}^{(i)}(u)$ and $\mathcal{F}_t(u)$ allow the heterogeneity being time-varying.

2.3.2 Dimension reduction on infinite dimensional functions

Once the dimensional reduced functional time series $\{\mathcal{F}_t^\top(u), t = 1, \dots, T\}$ are obtained, a functional factor model can be applied, such that

$$(2.3) \quad \mathcal{F}_t^\top(u) = \phi(u)\mathbf{F}_t + \mathbf{v}_t(u), \quad t = 1, 2, \dots, T,$$

where $\phi(u)$, the common functional loading, is a vector of length r ; \mathbf{F}_t is an $r \times k$ matrix and $\mathbf{v}_t(u)$ is also the white noise idiosyncratic component. By doing this, all the temporal dynamics are

reflected in the matrix-valued time series $\{\mathbf{F}_t\}$.

Combining (2.2) and (2.3), we can obtain the proposed model as in (2.1). The HDFTS $\mathcal{Y}_t(u) = [\mathcal{Y}_t^1(u), \dots, \mathcal{Y}_t^N(u)]^\top$ can also be expressed in a matrix format,

$$(2.4) \quad \mathcal{Y}_t(u) = \phi(u) \mathbf{F}_t \mathbf{\Lambda}^\top(u) + \epsilon_t(u), \quad t = 1, 2, \dots, T,$$

where $\mathbf{\Lambda}(u)$, the systems of back functional factor loadings, is an $N \times k$ back functional factor loading matrix ($k \ll N$), with the i^{th} row being $\lambda^{(i)}(u)$; and $\epsilon_t(u)$ is an N -dimensional vector of the white noise processes.

To understand the model better, we can extend the first component on the right-hand side of (2.4) as

$$(2.5) \quad \begin{aligned} \phi(u) \mathbf{F}_t \mathbf{\Lambda}^\top(u) &= \begin{bmatrix} \phi_1(u) & \phi_2(u) & \dots & \phi_r(u) \end{bmatrix} \begin{bmatrix} F_{t,11} & F_{t,12} & \dots & F_{t,1k} \\ F_{t,21} & F_{t,22} & \dots & F_{t,2k} \\ \vdots & \vdots & \ddots & \vdots \\ F_{t,r1} & F_{t,r2} & \dots & F_{t,rk} \end{bmatrix} \begin{bmatrix} \lambda_1^{(1)}(u) & \lambda_1^{(2)}(u) & \dots & \lambda_1^{(N)}(u) \\ \lambda_2^{(1)}(u) & \lambda_2^{(2)}(u) & \dots & \lambda_2^{(N)}(u) \\ \vdots & \vdots & \ddots & \vdots \\ \lambda_k^{(1)}(u) & \lambda_k^{(2)}(u) & \dots & \lambda_k^{(N)}(u) \end{bmatrix} \\ &= \left[\sum_{p=1}^r \sum_{q=1}^k \phi_p(u) F_{t,pq} \lambda_q^{(1)}(u) \quad \sum_{p=1}^r \sum_{q=1}^k \phi_p(u) F_{t,pq} \lambda_q^{(2)}(u) \quad \dots \quad \sum_{p=1}^r \sum_{q=1}^k \phi_p(u) F_{t,pq} \lambda_q^{(N)}(u) \right] \end{aligned}$$

where $\phi(u)$ is the loading curves common to all cross-sections. $\mathbf{\Lambda}(u)$ is the system loading curves specific to different cross-sections. By reducing the dimensions of both functional continuum and cross-sections, we can extract the important information of the HDFTS into an $r \times k \times T$ factor array \mathbf{F} . This array forms a matrix-valued time series, $\{\mathbf{F}_t, t = 1, 2, \dots, T\}$, which contains all the temporal dynamics of the high-dimensional functional series.

2.3.3 Connections with other existing models

The generality of the proposed model lies in the flexibility of the choice of the front and back loading functions. The connections with other existing models are discussed here.

Case 1 (Additive Fixed-Effect Model, Di et al. (2009)): Setting each entry in the back loading being the same constant function, i.e., $\lambda_q^{(i)}(u) = c$ for all $q \in 1, 2, \dots, k$ and $i \in 1, 2, \dots, N$. Equation (2.5) can be reduced as

$$\phi(u) \mathbf{F}_t \mathbf{\Lambda}^\top(u) = \left[\sum_{p=1}^r \phi_p(u) \sum_{q=1}^k c F_{t,pq} \quad \sum_{p=1}^r \phi_p(u) \sum_{q=1}^k c F_{t,pq} \quad \dots \quad \sum_{p=1}^r \phi_p(u) \sum_{q=1}^k c F_{t,pq} \right]$$

Let $\beta_{t,p} = \sum_{q=1}^k c_{F_{t,pq}}$, then $\mathcal{X}_t^{(i)}(u)$ can be expressed as

$$\mathcal{X}_t^{(i)}(u) = \mu^{(i)}(u) + \sum_{p=1}^r \beta_{t,p} \phi_p(u) + E_t^{(i)}(u), \quad t = 1, 2, \dots, T,$$

where $E_t^{(i)}(u)$ is the error component, for the ease of notation, we will use $E_t^{(i)}(u)$ to represent the error component for different models described below. This is the special case of functional panel data model with additive fixed effects of [Di et al. \(2009\)](#), where is no component for the cross-section, i .

Case 2 (Multivariate, Ramsay and Silverman (2006)): If we set each entry in the back loading matrix being a constant function specific to each i , i.e., $\lambda_q^{(i)}(u) = c_i$, for all $q \in 1, 2, \dots, k$. Equation (2.5) can be reduced as

$$\phi(u) \mathbf{F}_t \mathbf{\Lambda}^\top(u) = \left[\sum_{p=1}^r \phi_p(u) \sum_{q=1}^k c_{1F_{t,pq}} \quad \sum_{p=1}^r \phi_p(u) \sum_{q=1}^k c_{2F_{t,pq}} \quad \dots \quad \sum_{p=1}^r \phi_p(u) \sum_{q=1}^k c_{NF_{t,pq}} \right]$$

Let $\beta_{t,p}^{(i)} = \sum_{q=1}^k c_i F_{t,pq}$, then $\mathcal{X}_t^{(i)}(u)$ can be expressed as

$$\mathcal{X}_t^{(i)}(u) = \mu^{(i)}(u) + \sum_{p=1}^r \beta_{t,p}^{(i)} \phi_p(u) + E_t^{(i)}(u), \quad t = 1, 2, \dots, T,$$

the model becomes the Karhunen-Loève (KL) representation for multivariate functional data, where all functions from different cross-sections share the same bases.

Case 3 (High-Dimensional Factor Model, Nisol et al. (2019)): If we set each entry in the back loading matrix being a function specific to i , i.e., $\lambda_q^{(i)}(u) = \gamma^{(i)}(u)$, for all $q \in 1, 2, \dots, k$. Equation (2.5) can be reduced as

$$\phi(u) \mathbf{F}_t \mathbf{\Lambda}^\top(u) = \left[\sum_{p=1}^r \gamma^{(1)}(u) \phi_p(u) \sum_{q=1}^k F_{t,pq} \quad \sum_{p=1}^r \gamma^{(2)}(u) \phi_p(u) \sum_{q=1}^k F_{t,pq} \quad \dots \quad \sum_{p=1}^r \gamma^{(N)}(u) \phi_p(u) \sum_{q=1}^k F_{t,pq} \right]$$

Let $\beta_{t,p} = \sum_{q=1}^k F_{t,pq}$ and $\phi_p^{(i)}(u) = \gamma^{(i)}(u) \phi_p(u)$, $\mathcal{X}_t^{(i)}(u)$ can be expressed as

$$\mathcal{X}_t^{(i)}(u) = \mu^{(i)}(u) + \sum_{p=1}^r \beta_{t,p} \phi_p^{(i)}(u) + E_t^{(i)}(u), \quad t = 1, 2, \dots, T,$$

then it is the high-dimensional factor model of [Nisol et al. \(2019\)](#). Similarly, we can obtain the same model if the front loading is set to be a constant scalar, i.e., $\phi_p(u) = c$.

Case 4 (Individual FPCA, Gao et al. (2019)): If we set each entry in the front loading being a constant specific to i for $i = 1, 2, \dots, N$, i.e., $\phi_p(u) = c_i$ for all $p = 1, 2, \dots, r$. Equation (2.5) can be re-expressed as

$$\phi(u)\mathbf{F}_t\mathbf{\Lambda}^\top(u) = \left[\sum_{q=1}^k \lambda_q^{(1)}(u) \sum_{p=1}^r c_{1F_t,pq} \quad \sum_{q=1}^k \lambda_q^{(2)}(u) \sum_{p=1}^r c_{2F_t,pq} \quad \dots \quad \sum_{q=1}^k \lambda_q^{(N)}(u) \sum_{p=1}^r c_{NF_t,pq} \right]$$

Let $\beta_{t,q}^{(i)} = \sum_{p=1}^r c_{iF_t,pq}$ and $\phi_q^{(i)}(u) = \lambda_q^{(i)}(u)$, $\mathcal{X}_t^{(i)}(u)$ can be expressed as

$$\mathcal{X}_t^{(i)}(u) = \mu^{(i)}(u) + \sum_{q=1}^k \beta_{t,q}^{(i)} \phi_q^{(i)}(u) + E_t^{(i)}(u), \quad t = 1, 2, \dots, T,$$

then it is the KL representation for univariate functional data, from which the factor model of Gao et al. (2019) is derived.

Case 5 (Matrix Factor Model, Wang et al. (2019)): If we discretize the functional continuum u into grid points and consider the discrete high-dimensional setting rather than functional setting, and set each entry in the back loading matrix being a different scalar, i.e., $\lambda_q^{(i)}(u) = c_{i,q}$, and then it is equivalent to the factor model for matrix-values high-dimensional time series of Wang et al. (2019).

3 Estimation

In this subsection, the estimation procedures for $\{\mu^{(i)}(u), \phi(u), \mathbf{F}_t, \mathbf{\Lambda}(u)\}$ in (2.1) are presented in detail. In general, the idea of the estimation procedure is to estimate the systems of back loadings first so that the HDFTS is reduced to functional time series of lower dimensions. Then the common front loading and the matrix-valued time series, $\{\mathbf{F}_t : t = 1, \dots, T\}$.

Suppose we have T curves in each cross-section, the estimation of $\mu^{(i)}(u)$ is as follows

$$\widehat{\mu}^{(i)}(u) = \frac{1}{T} \sum_{t=1}^T \mathcal{X}_t^{(i)}(u).$$

Then $\mathcal{Y}_t^{(i)}(u)$ is estimated as

$$\widehat{\mathcal{Y}}_t^{(i)}(u) = \mathcal{X}_t^{(i)}(u) - \widehat{\mu}^{(i)}(u).$$

3.1 Estimation of functional loadings $\Lambda(\mathbf{u})$

According to the model, the cross-section specific functional loadings, $\{\lambda^{(i)}(\mathbf{u})\}$, represent the heterogeneity of each set of functional time series, each row can be estimated individually. To accommodate the serial dependence in each cross-section, the i^{th} row of $\Lambda(\mathbf{u})$, $\lambda^{(i)}(\mathbf{u})$ is estimated by the eigendecomposition of the long-run covariance operator corresponding to the i^{th} cross-section. This refers to dynamic functional principal component analysis (FPCA), which is described below.

Given the incapability of classic FPCA in accounting for the essential information provided by the serial dependence structure in functional time series, dynamic FPCA is developed. [Horváth et al. \(2013\)](#) and [Panaretos and Tavakoli \(2013b\)](#) define smoothed periodogram type estimates of the long-run covariance and spectral density operators for functional time series. [Hörmann et al. \(2015\)](#) use the spectral density operator to create functional filters to construct mutually uncorrelated dynamic FPCs so that the dynamic FPC scores can be analyzed component-wisely. [Rice and Shang \(2017\)](#) propose a bandwidth selection method for estimates of the long-run covariance function based on finite-order weight functions that aim to minimize the estimator's asymptotic mean-squared normed error. Following their work, the long-run covariance function for the i^{th} cross-section $c^{(i)}(u, v)$ can be estimated by

$$\hat{c}^{(i)}(u, v) = \sum_{s=-\infty}^{\infty} W\left(\frac{s}{H}\right) \hat{c}_s^{(i)}(u, v),$$

where

$$\hat{c}_s^{(i)}(u, v) = \begin{cases} \frac{1}{T-s} \sum_{t=1}^{T-s} \hat{\mathcal{Y}}_t^{(i)}(u) \hat{\mathcal{Y}}_{t+s}^{(i)}(v), & s \geq 0; \\ \frac{1}{T-s} \sum_{t=1-s}^T \hat{\mathcal{Y}}_t^{(i)}(u) \hat{\mathcal{Y}}_{t+s}^{(i)}(v), & s < 0. \end{cases}$$

$W(\cdot)$ is the kernel function that assigns different weights to the auto-covariance functions of different lags, and H is the bandwidth. Despite many different types of kernel functions (see [Hansen, 1982](#); [White, 1984](#); [Newey and West, 1987](#); [Andrews, 1991](#); [Gallant, 2009](#), for types of kernel functions), the common nature is to assign more weights to the auto-covariance functions of small lags and less weight to the auto-covariance functions of large lags. Here we use flat-top kernel functions as they give a reduced bias and faster rates of convergence ([Politis and Romano, 1996](#),

1999). Flat-top kernels are of the following form

$$W\left(\frac{s}{H}\right) = \begin{cases} 1, & 0 \leq \left|\frac{s}{H}\right| < \nu; \\ \frac{\left|\frac{s}{H}\right|-1}{\nu-1}, & 0 \leq \left|\frac{s}{H}\right| < 1; \\ 0, & \left|\frac{s}{H}\right| \geq 1, \end{cases}$$

where $\nu < 1$. The choice of the bandwidth can greatly affect the finite-sample performance. Therefore, we apply the adaptive bandwidth selection procedure of [Rice and Shang \(2017\)](#) to gain a better estimate of the long-run covariance functions.

The long-run covariance operator can be estimated by

$$\widehat{C}^{(i)}(y)(u) = \sum_{s=-\infty}^{\infty} W\left(\frac{s}{H}\right) \widehat{C}_s^{(i)}(y)(u),$$

where $\widehat{C}_s^{(i)}(y)(u) = \int_{\mathcal{I}} \widehat{c}_s^{(i)}(u, v) y(v) dv$, is the sample covariance operator at lag s .

The estimates of $\lambda^{(i)}(\mathbf{u})$, $\widehat{\lambda}^{(i)}(\mathbf{u}) = [\widehat{\lambda}_1^{(i)}(\mathbf{u}), \dots, \widehat{\lambda}_{k_i}^{(i)}(\mathbf{u})]$ are the eigenfunctions corresponding to the first k_i largest eigenvalues of $\widehat{C}^{(i)}(y)(u)$. Since we allow the $\lambda^{(i)}(\mathbf{u})$ to vary according to i , it represents the heterogeneity of each cross-section.

To maintain the matrix format of the loadings of each cross-section, k is selected to be

$$k = \max\{k_i : 1 \leq i \leq N\},$$

where $k_i, i = 1, \dots, N$ is the optimal the numbers of components used for i^{th} cross-section.

Selecting the optimal number of functional principal components has been well studied in the literature ([Rice and Silverman, 1991](#); [Yao et al., 2005](#); [Hall and Vial, 2006](#); [Chiou, 2012](#); [Hörmann and Kidziński, 2015](#)). In this paper, k_i is determined by the cumulative percentage of variance method ([Chiou, 2012](#)), such that

$$(3.6) \quad k_i = \operatorname{argmin}_{k_i: k_i \geq 1} \left(\frac{\sum_{m=1}^{k_i} \widehat{\lambda}_m^{(i)}}{\sum_{m=1}^{\infty} \widehat{\lambda}_m^{(i)} \mathbb{1}\{\widehat{\lambda}_m^{(i)} > 0\}} \geq P \right),$$

where $\lambda_m^{(i)}$ is the m^{th} largest eigenvalue of $\widehat{C}^{(i)}(y)(u)$, $\mathbb{1}\{\cdot\}$ denotes the binary indicator function and P is a predetermined value and is chosen to be 0.9 (see, e.g., [Horváth and Kokoszka, 2012](#)).

3.2 Estimation of $\mathcal{F}_t(u)$

In order to estimate $\phi(\mathbf{u})$ and F_t , we need to estimate $\mathcal{F}_t(u)$ in (2.2), i.e., extract the common features of the HDFTS. Expressing (2.2) in matrix format,

$$\mathbf{y}_t(u) = \Lambda(u)\mathcal{F}_t(u) + \epsilon_t(u), \quad t = 1, 2, \dots, T,$$

where $\Lambda(u)$ is an $N \times k$ matrix of functions and $\mathcal{F}_t(u)$ is a $k \times 1$ vector of functions. The i^{th} entry of $\mathbf{y}_t(u)$ can be expressed as follows:

$$y_t^{(i)}(u) = \sum_{q=1}^k \lambda_q^{(i)}(u)\mathcal{F}_{t,q}(u) + \epsilon_t^{(i)}(u).$$

This is essentially the functional concurrent regression model in Ramsay et al. (2009), but without intercept function, where $\lambda_q^{(i)}(u)$ is a k -dimensional functional observation and $\mathcal{F}_{t,q}(u)$ is the functional regression coefficients.

Let the N -dimensional residual functions vector being

$$\mathbf{r}_t(u) = \mathbf{y}_t(u) - \Lambda(u)\mathcal{F}_t(u),$$

$\mathcal{F}_t(u)$ can be estimated through minimizing the penalized sum of squares, such that

$$(3.7) \quad \hat{\mathcal{F}}_t(u) = \underset{\mathcal{F}_t(u)}{\operatorname{argmin}} \left(\int \mathbf{r}_t(u)^\top \mathbf{r}_t(u) du + \sum_{q=1}^k \gamma_q \int [L_q \mathcal{F}_{t,q}(u)]^2 du \right),$$

where γ_q is the smoothing parameter and $L_q \mathcal{F}_{t,q}(u)$ is the linear differential operator applied to $\mathcal{F}_{t,q}(u)$, γ_q and $L_q \mathcal{F}_{t,q}(u)$ define the roughness penalty together.

Functional concurrent regression is performed for each $t = 1, 2, \dots, T$, such that $\hat{\mathcal{F}}(u) = [\hat{\mathcal{F}}_1(u)^\top, \hat{\mathcal{F}}_2(u)^\top, \dots, \hat{\mathcal{F}}_T(u)^\top]^\top$ is a matrix of function-valued objects, each with a dimension of $T \times k$, we have a panel of dimension-reduced functional time series, which represents the common features.

3.3 Estimation of the front functional loading $\phi(u)$ and factor matrix F_t

Once $\widehat{\mathcal{F}}(u)$ is obtained, we can estimate $\phi(u)$ and F_t based on (2.3). Since $\mathcal{F}(u)$ is a dimension-reduced panel of functional time series, where each column may be correlated, therefore, the key is to calculate the auto-cross-covariance of $\mathcal{F}(u)$. Wang et al. (2019) use the auto-cross-covariance to capture the co-movement observations from different cross-sections of different lags. We here extend it to the functional version. Let $C_{h,lj}(u, v)$ being the auto-cross-covariance function of the l^{th} and j^{th} column of $\mathcal{F}(u)$, for l and $j = 1, \dots, k$, such that

$$C_{h,lj}(u, v) = \text{Cov} \left[\mathcal{F}_{t,l}(u), \mathcal{F}_{t+h,j}(u) \right].$$

Since the operator using $C_{h,lj}(u, v)$ as a kernel is not nonnegative, we define a nonnegative operator (using a similar idea as Bathia et al., 2010),

$$M_{h,lj}(u, v) = \int_{\mathcal{I}} C_{h,lj}(u, z) C_{h,lj}(v, z) dz.$$

Then for a predetermined integer h_0 , the operator

$$(3.8) \quad M(u, v) = \sum_{h=1}^{h_0} \sum_{l=1}^k \sum_{j=1}^k M_{h,lj}(u, v),$$

is also nonnegative. The auto-cross-covariance function can be estimated by

$$\widehat{C}_{h,lj}(u, v) = \frac{1}{T-h} \sum_{t=1}^{T-h} \widehat{\mathcal{F}}_{t,l}(u) \widehat{\mathcal{F}}_{t+h,j}(v).$$

Hence, the operator $M(u, v)$ can be estimated by

$$\widehat{M}(u, v) = \sum_{h=1}^{h_0} \sum_{l=1}^k \sum_{j=1}^k \int_{\mathcal{I}} \widehat{C}_{h,lj}(u, z) \widehat{C}_{h,lj}(v, z) dz.$$

The estimates of $\phi(u)$, $\widehat{\phi}(u) = [\widehat{\phi}_1(u), \dots, \widehat{\phi}_r(u)]$ are the eigenfunctions corresponds to the first r largest eigenvalues of the eigendecomposition on $\widehat{M}(u, v)$. The optimal r can be selected using a same approach as in (3.6).

Once $\widehat{\phi}(u)$ is obtained, the estimated $\widehat{\mathbf{F}}_t$ can be obtained through

$$\widehat{\mathbf{F}}_t = \int_{\mathcal{I}} \widehat{\phi}(u)^\top \widehat{\mathcal{F}}_t(u)^\top du,$$

where $\widehat{\mathbf{F}}_t$ is an $r \times k$ matrix. Therefore, all the temporal information is extracted into the T sheets of $r \times k$ matrices.

In summary, we first separate out the heterogeneity among the HDFTS, where a specific set of functional loading, $\widehat{\lambda}^{(i)}(u)$, is obtained for each set of functional time series. The common features can then be extracted into functional time series of smaller dimensions, $\widehat{\mathcal{F}}_t(u)$. Then functional dynamic factor model is applied to the dimension-reduced functional time series, $\widehat{\mathcal{F}}_t(u)$, such that all the temporal information can be extracted into the matrix-valued time series $\{\widehat{\mathbf{F}}_t : t = 1, \dots, T\}$.

4 Forecasting

Based on the proposed model, the information contained in the original panel of functional time series is extracted into T sheets of fixed dimensional factor matrices, \mathbf{F}_t . Forecasting the high-dimensional functional times series is equivalent to forecasting the estimated factor matrices, $\widehat{\mathbf{F}}_t$, for $t = 1, 2, \dots, T$. The h -step-ahead in sample forecast of the estimated factors, $\widehat{\mathbf{F}}_{\kappa+h|\kappa}$ can be obtained by fitting a Vector Autoregressive (VAR) model to the estimated factors $\{\widehat{\mathbf{F}}_1, \widehat{\mathbf{F}}_2, \dots, \widehat{\mathbf{F}}_\kappa\}^\top$, where $\kappa < T$ is the size of the sample used for forecasting. In selecting the order of VAR model, we follow the method of [Tsay \(2013\)](#), where he uses the information criterion approach, here we use the Akaike information criterion (AIC).

For a given sample size κ , the h -step-ahead in sample forecast of the i^{th} cross-section in the HDFTS can be calculated as

$$\widehat{\mathcal{X}}_{\kappa+h|\kappa}^{(i)}(u) = \widehat{\mu}^{(i)}(u) + \widehat{\phi}(u) \widehat{\mathbf{F}}_{\kappa+h|\kappa} \widehat{\lambda}^{(i)}(u).$$

To capture the uncertainties in the point forecasts, prediction intervals for functions could also be constructed. We apply the nonparametric bootstrap approach of [Shang \(2018\)](#) in constructing point-wise prediction intervals for functions.

For a grid point u_j on the curve, the h -step-ahead bootstrapped forecasts of the i^{th} cross-section, $\widehat{\mathcal{X}}_{\kappa+h|\kappa}^{(i),b}(u_j)$, can be obtained by adding a bootstrapped residual, $\widehat{e}_{\kappa+h|\kappa}^{(i),b}(u_j)$ to the point forecast,

$\widehat{\mathcal{X}}_{\kappa+h|\kappa}^{(i)}(u_j)$, where $\widehat{e}_{\kappa+h|\kappa}^{(i),b}(u_j)$ is generated using sampling with replacement from the in-sample-forecast errors, $\widehat{e}_{\kappa+h|\kappa}^{(i)}(u_j) = \mathcal{X}_{\kappa+h}^{(i)}(u_j) - \widehat{\mathcal{X}}_{\kappa+h|\kappa}^{(i)}(u_j)$. For a given significance level α , the h -step-ahead bootstrapped point-wise prediction interval for the i^{th} cross-section, $\left[\widehat{\mathcal{X}}_{\kappa+h|\kappa}^{(i),\text{lb}}(u_j), \widehat{\mathcal{X}}_{\kappa+h|\kappa}^{(i),\text{ub}}(u_j) \right]$, can be calculated point-wisely as the $100 \times (\alpha/2)^{\text{th}}$ and $100 \times (1 - \alpha/2)^{\text{th}}$ percentile of the bootstrapped forecasts at each grid point, respectively. The estimation procedure and the forecasting method are summarized in Algorithm 1.

Algorithm 1: High-dimensional functional time series forecasting

1 **Input:** High-dimensional functional time series $\{ \mathcal{X}_t(u) = [\mathcal{X}_t^{(1)}, \mathcal{X}_t^{(2)}, \dots, \mathcal{X}_t^{(N)}], t = 1, \dots, \kappa \}$.

2 **1. Estimation Step:**

1.1 For $i \in \{1, \dots, N\}$, compute the sample mean $\widehat{\mu}^{(i)} = \frac{1}{\kappa} \sum_{t=1}^{\kappa} \mathcal{X}_t^{(i)}(u)$;

1.2 For $i \in \{1, \dots, N\}$, compute the demeaned function $\widehat{\mathcal{Y}}_t^{(i)} = \mathcal{X}_t^{(i)}(u) - \widehat{\mu}^{(i)}$;

1.3 For $i \in \{1, \dots, N\}$, perform dynamic FPCA to $\widehat{\mathcal{Y}}^{(i)} = [\widehat{\mathcal{Y}}_1^{(i)}, \widehat{\mathcal{Y}}_2^{(i)}, \dots, \widehat{\mathcal{Y}}_{\kappa}^{(i)}]^{\top}$ and obtain the eigenfunctions $\widehat{\lambda}^{(i)}(\mathbf{u}) = [\widehat{\lambda}_1^{(i)}(u), \dots, \widehat{\lambda}_{k_i}^{(i)}(u)]$ corresponding to the first k_i largest eigenvalues of the long-run covariance operator of $\widehat{\mathcal{Y}}_t^{(i)}$, where k_i is selected based on (3.6);

1.4 Choose $k = \max\{k_i : 1 \leq i \leq N\}$, such that the loadings of each cross-section are of the same dimension such that $\Lambda(u) = [\widehat{\lambda}^{(1)}(u), \widehat{\lambda}^{(2)}(u), \dots, \widehat{\lambda}^{(N)}(u)]^{\top}$;

1.5 For $t \in \{1, \dots, \kappa\}$, perform the concurrent functional regression with $\{\widehat{\mathcal{Y}}_t^{(i)}, i = 1, \dots, N\}$ as the response and $\{\widehat{\lambda}^{(i)}(u), i = 1, \dots, N\}$ as covariates and obtain the coefficient functions $\widehat{\mathcal{F}}_t(u) = [\widehat{\mathcal{F}}_{t,1}(u), \dots, \widehat{\mathcal{F}}_{t,k}(u)]$;

1.6 $\widehat{\mathcal{F}}(u) = [\widehat{\mathcal{F}}_1(u)^{\top}, \widehat{\mathcal{F}}_2(u)^{\top}, \dots, \widehat{\mathcal{F}}_T(u)^{\top}]^{\top}$;

1.6 For $i, j \in \{1, \dots, k\}$, compute $\widehat{C}_{h,lj}(u, v) = \frac{1}{T-h} \sum_{t=1}^{T-h} \widehat{\mathcal{F}}_{t,l}(u) \widehat{\mathcal{F}}_{t+h,j}(v)$;

1.7 For a predetermined h_0 , compute $\widehat{M}(u, v) = \sum_{h=1}^{h_0} \sum_{l=1}^k \sum_{j=1}^k \int_{\mathcal{I}} \widehat{C}_{h,lj}(u, z) \widehat{C}_{h,lj}(v, z) dz$;

1.8 Conduct eigen-decomposition on $\widehat{M}(u, v)$ and get $\widehat{\phi}(u) = [\widehat{\phi}_1(u), \dots, \widehat{\phi}_r(u)]$, the eigenfunctions corresponding to the first r largest eigenvalues of $\widehat{M}(u, v)$, where r is selected based on similar idea as in (3.6);

1.9 For $t \in \{1, \dots, \kappa\}$, compute $\widehat{\mathbf{F}}_t = \int_{\mathcal{I}} \widehat{\phi}(u)^{\top} \widehat{\mathcal{F}}_t(u)^{\top} du$.

2. **Forecasting Step:**

2.1 Obtain the h -step ahead forecast of $\{\widehat{\mathbf{F}}_t, t = 1, \dots, \kappa\}$, $\widehat{\mathbf{F}}_{\kappa+h|\kappa}$;

2.2 Recover the h -step-ahead forecast of the i^{th} cross-section of the high-dimensional functional time series, $\widehat{\mathcal{X}}_{\kappa+h|\kappa}^{(i)}(u) = \widehat{\mu}^{(i)}(u) + \widehat{\phi}(u) \widehat{\mathbf{F}}_{\kappa+h|\kappa} \widehat{\lambda}^{(i)}(u)$.

Result: $\widehat{\mathcal{X}}_{\kappa+h|\kappa}^{(i)}(u)$, the h -step-ahead forecast of the i^{th} cross-section of the high-dimensional functional time series.

5 Simulation studies

In this section, we use Monte Carlo simulations to evaluate the finite sample performance of the proposed model. The N sets of correlated functional time series are generated according to (2.1),

in particular, the t^{th} curve of the i^{th} functional time series is generated from the following model contaminated with measurement error $\epsilon_t^{(i)}(u)$

$$\mathcal{Y}_t^{(i)}(u) = \phi(u) \mathbf{F}_t \boldsymbol{\lambda}^{(i)}(u) + \epsilon_t^{(i)}(u), \quad t = 1, 2, \dots, T, \quad i = 1, 2, \dots, N,$$

where \mathbf{F}_t is a 2×2 matrix with the each row is generated using vector autoregressive model of order 1 (VAR(1)). Specifically, the first and second row are generated using VAR(1) model with coefficient matrix $\begin{pmatrix} 0.7 & 0.2 \\ 0.2 & 0.7 \end{pmatrix}$ and $\begin{pmatrix} 0.5 & -0.25 \\ -1 & 0.5 \end{pmatrix}$, respectively. The covariance matrix of the innovations for both VAR(1) models are $\begin{pmatrix} 1 & 0.5 \\ 0.5 & 1 \end{pmatrix}$. The two front loading curves are $\phi_1(u) = \sin(4\pi u)$ and $\phi_2(u) = \cos(4\pi u)$, respectively, with $\{u = \frac{m}{100} : m = 0, 1, \dots, 100\}$. The two back loading curves for each i are $\lambda_2^{(i)} = \sin(2\pi u + \pi i/4)$ and $\lambda_1^{(i)} = \cos(2\pi u + \pi i/4)$, respectively. The measurement error $\epsilon_t^{(i)}(u)$ is generated from independent and identically distributed $N(0, 0.5^2)$ for all i and u .

We generate data using different combinations of N and T . For each value of T , we chose N being $\frac{T}{2}$, T and $2T$. The predetermined integer h_0 in (3.8) is taken to be one as the VAR model is of order one.

The model fitting can be evaluated using root mean squared error (RMSE)

$$\text{RMSE}(h) = \sqrt{\frac{1}{N \times T \times 101} \sum_{i=1}^N \sum_{t=1}^T \sum_{m=1}^{101} [\mathcal{Y}_t^{(i)}(u_m) - \hat{\mathcal{Y}}_t^{(i)}(u_m)]^2},$$

where $\hat{\mathcal{Y}}_t^{(i)}(u_m)$ represents the estimated function value at grid points u_m for $m = 0, \dots, 100$. For each combination of N and T , we simulate 100 replications and compute the mean of the RMSE values.

Table 1 displays the model fitting performance, and it is obvious that for each N , when T increases, the estimation error is smaller, which is a common phenomenon as the sample size is larger. Similarly, for each T , as N , the dimension increases, the estimation error is stable, and the proportion of the corrected estimated number of factors significantly increases, which indicates that our model could handle high-dimensional cases when $N > T$.

We also compare the forecast performance of the proposed model with the univariate functional time series forecasting method of Hyndman and Ullah (2007). The simulated data is split into two sets in evaluating the forecasting performance, i.e., the training set and the testing set. Different models are fitted with the training dataset, and forecasts are made based on different models. Then

Table 1: Estimation performance for different combinations of N and T . RMSE measures the model fitting and \hat{r} and \hat{k} , measure the proportion of the correctly estimated number of front-loading curves and back loading curves.

T	N	RMSE	$\hat{r} = 2 \text{ or } 3$	$\hat{k} = 2$
20	10	1.21	0.36	0.88
	20	1.14	0.44	0.90
	40	1.25	0.60	0.94
40	20	1.12	0.66	0.93
	40	0.99	0.73	0.96
	80	1.07	0.82	0.98

the forecasts are compared with the actual observations in the testing set. In this case, we set the starting size of the training set and testing set is $\lfloor \frac{3}{4} \times T \rfloor$ and $\lceil \frac{1}{4} \times T \rceil$, respectively. We use the expanding window analysis, where each time we increase the training size by one and refit the models. We obtain the one- to five-step ahead forecasts and compute our forecasts' root mean square forecast error (RMSFE).

$$\text{RMSFE}(h) = \sqrt{\frac{1}{N \times (\frac{1}{4} \times T - h + 1) \times 101} \sum_{i=1}^N \sum_{\kappa=\frac{3}{4} \times T}^{T-h} \sum_{m=1}^{101} [\mathcal{Y}_{\kappa+h}^{(i)}(u_m) - \hat{\mathcal{Y}}_{\kappa+h|\kappa}^{(i)}(u_m)]^2},$$

where κ is the size of the data used to generate forecast and $\hat{\mathcal{Y}}_{\kappa+h|\kappa}^{(i)}(u_m)$ represents the forecast values at grid points u_m for $m = 0, \dots, 100$.

For each combination of N and T , we simulate 100 replications and compute the mean of the RMSFE values of different models. Table 2 shows the mean RMSFE values for different combinations of N and T for both models. The bold entries highlight the method that produces the most accurate forecast. The proposed model produces a more accurate forecast for almost most of the cases for all the combinations of N and T , demonstrating the proposed model's superiority in forecasting HDFTS.

Table 2: The mean of RMSFE values of different models for different combinations of N and T , "FVP" represents the proposed model and "UFTS" represents the univariate functional time series forecasting model.

		$N = 10$		$N = 20$		$N = 40$	
T	h	UFTS	FVP	UFTS	FVP	UFTS	FVP
20	1	1.739	1.424	1.459	1.623	1.447	1.878
	2	1.851	1.614	1.701	1.640	1.839	1.921
	3	1.931	1.840	2.026	1.729	2.045	1.901
	4	1.882	1.772	2.248	1.711	2.454	2.045
	5	2.132	1.957	2.264	1.779	2.724	2.068
		$N = 20$		$N = 40$		$N = 80$	
	h	UFTS	FVP	UFTS	FVP	UFTS	FVP
40	1	2.189	1.381	2.647	1.478	2.758	1.555
	2	2.276	1.661	2.743	1.862	2.856	1.958
	3	2.362	1.858	2.841	2.141	2.977	2.223
	4	2.447	2.091	2.956	2.301	3.008	2.356
	5	2.493	2.202	3.131	2.530	3.184	2.589

6 Empirical Studies

We apply the proposed method to forecast the sub-national mortality rates in Japan ([Japan Mortality Database, 2021](#)). The data contains the age-specific mortality rates of 47 prefectures of Japan from 1975 to 2015. Due to the sparsity of the data at very high age, we have aggregated the female mortality for ages over 100, and male mortality for ages over 98, hence the numbers of grid points on the mortality curves for female and male mortality are 101 and 99, respectively. In this section, we compare the forecasting accuracy of the proposed method with several competing methods. Further, we use life annuity pricing to demonstrate the impact of the forecasting improvement brought by the proposed method.

6.1 Japanese mortality data

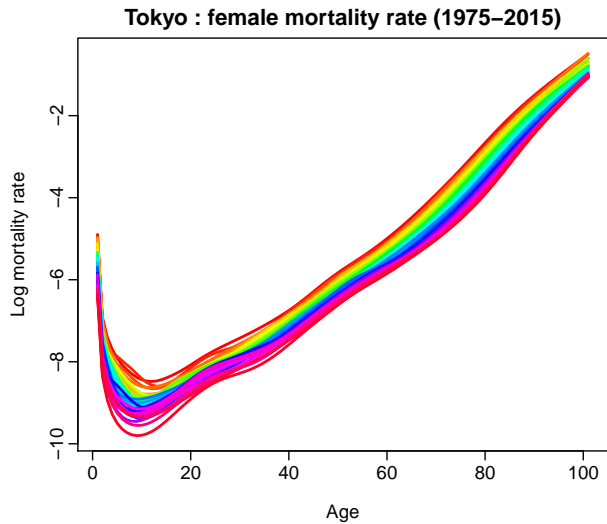
Hyndman and Shang (2010) develop rainbow plots to visualize functional time series. The color order of the rainbow reflects the time ordering of the functional time series. Functions from earlier times are in red, and those from more recent times are in purple. Figure 1 depicts the rainbow plots of the logarithm of the smoothed female mortality rates for four prefectures of Japan, namely, Tokyo, Nagano, Kyoto, and Osaka, from 1975 to 2015. Despite the general shapes of mortality rates for these four prefectures being similar, we may observe significant differences in the troughs and peaks and the overlaps of the curves. This means the mortality rates of different prefectures contain heterogeneity. Therefore, to achieve improved forecasts of the mortality rates, which is high-dimensional, we need to extract the common features and use these common features to produce forecasts. This could be achieved by separating the homogeneity and heterogeneity of mortality rates of all prefectures. As indicated in model (2.4), the heterogeneity of mortality rates of each prefecture is reflected in $\Lambda(u)$, the $N \times k$ functional factor loading matrix, since each country has a different set of functional factor loading. While the term $\phi(u)F_t$ represents the homogeneity, which is common to all functional time series.

Figure 2 shows the first four functional factor loadings of mortality rates of these four prefectures. All these four-factor loadings are different for these four prefectures; this represents the heterogeneity in the mortality rates, more specifically, the different troughs, peaks, and overlaps of the mortality rate curves of these prefectures.

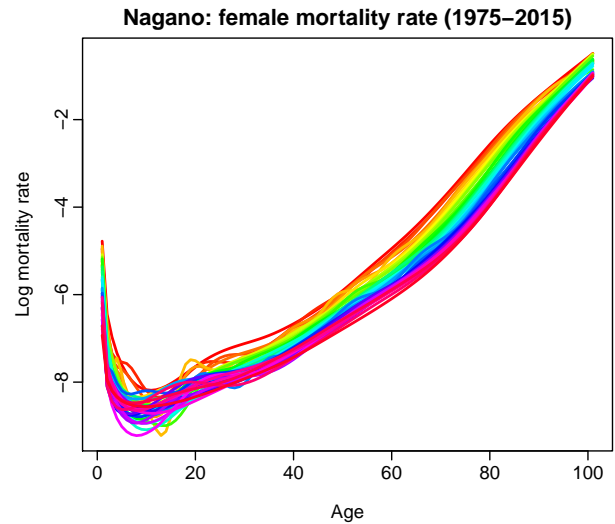
After separating the heterogeneity, we have extracted the common features displayed in Figure 3, which is common to all mortality rates curves. This reflects the general common shapes and color ordering of the mortality rates of all prefectures of Japan. By extracting the common features, we have reduced the dimension of the functional time series of 47 prefectures of Japan into smaller sets of functional time series. The temporal information within the original HDFTS is preserved in the fixed-dimensional functional time series. In addition, the first four common functional factor loadings of both genders are depicted in Figure 4.

Table 3 reports the first six eigenvalues¹ for the auto-cross-covariance function of the common functional time series and the long-run-covariance function of the functional time series of 4 selected prefectures of both genders. The eigenvalues are normalized so that the sum of all eigenvalues adds up to one to reflect the percentage of total variation explained. We observe that the first few

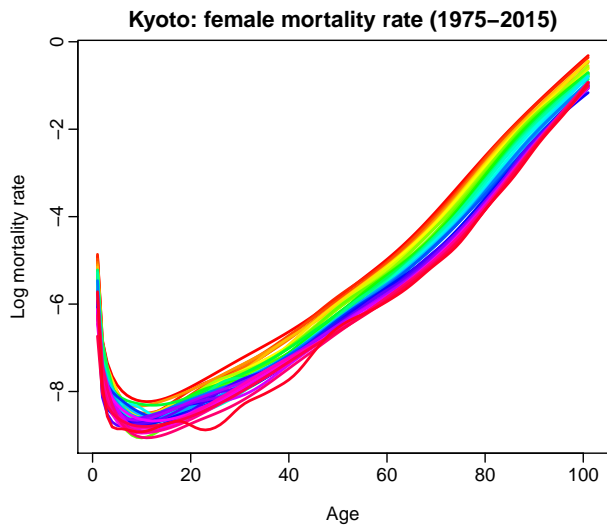
¹Eigenvalues are reported in descending order.



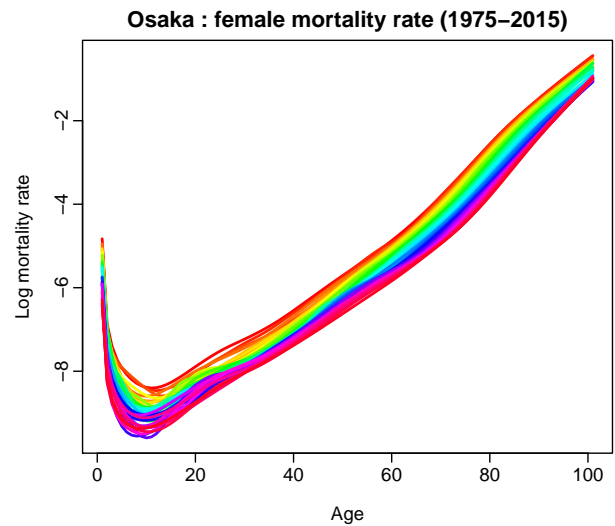
(a) Female smoothed mortality rates in Tokyo



(b) Female smoothed mortality rates in Nagano



(c) Female smoothed mortality rates in Kyoto



(d) Female smoothed mortality rates in Osaka

Figure 1: Functional time series displays for smoothed age-specific mortality rates of selected prefectures in Japan.

factors would explain most of the variation of the data. The numbers of factors that we select for the common functional time series and specific functional time series are 4 and 6, respectively, for females and 7 and 8, respectively, for males. With these selections of the number of factors, we ensure that the factors explain 99% of the variation in the data. Moreover, the percentages of total variation explained by the first factor for males are smaller than those for females, and this is because the male data are more volatile.

Functional factor loadings for four prefectures

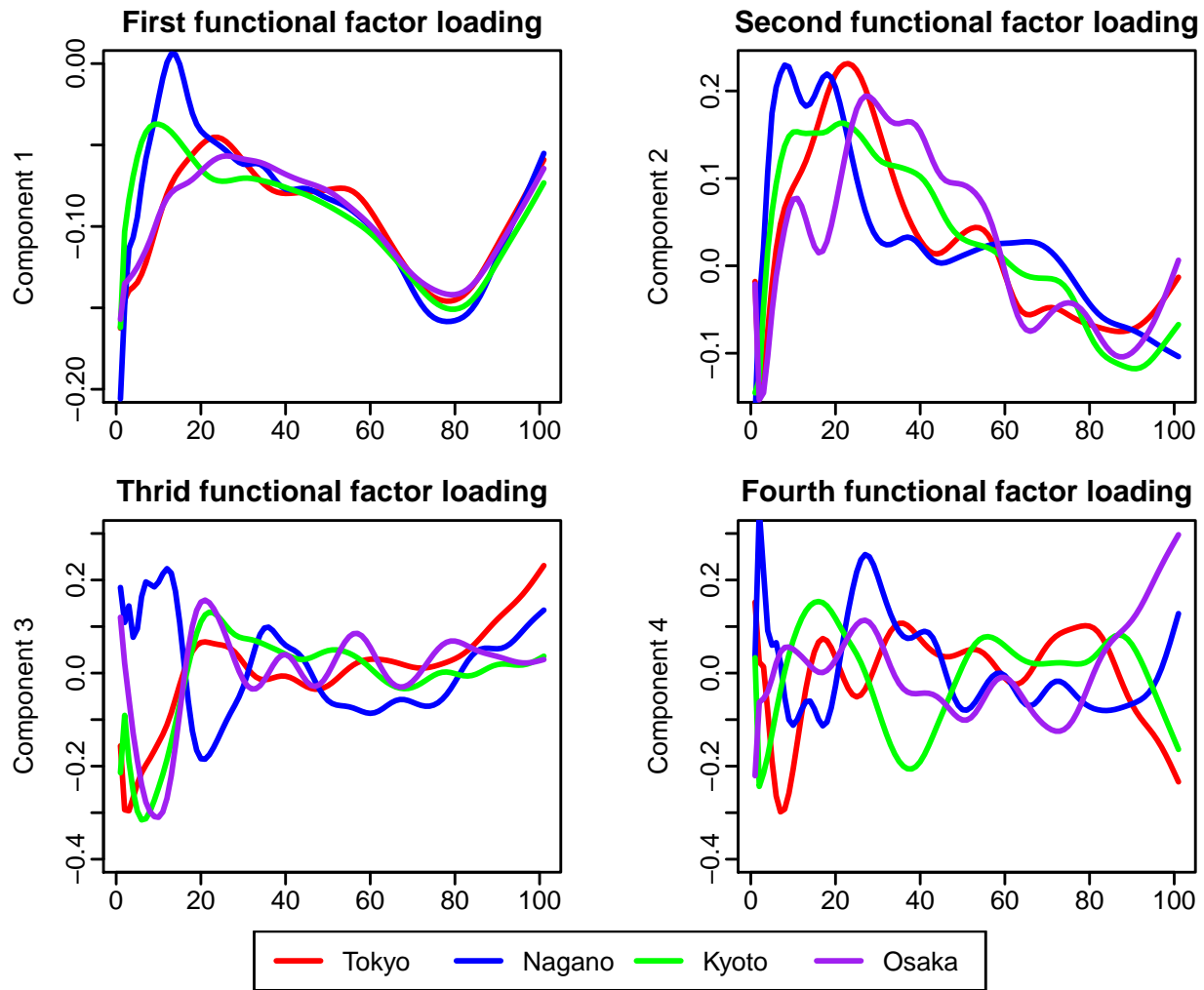
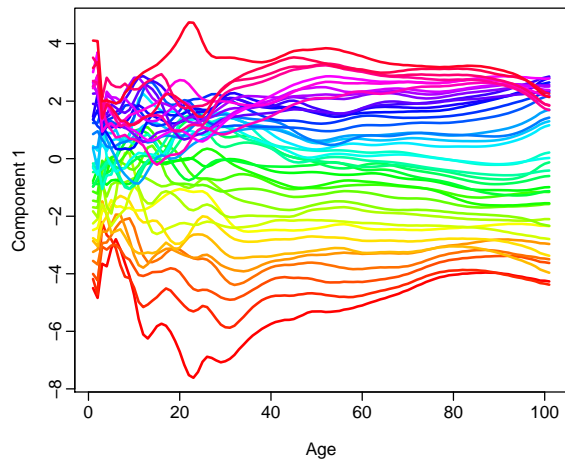


Figure 2: Country specific factor loadings for four prefectures of Japan.

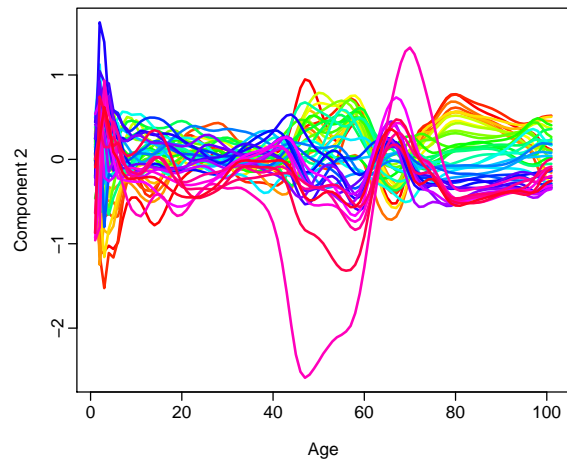
6.2 Forecast evaluation

To generate forecasts, a functional version of factor analysis can be performed to extract the temporal information into factor matrices $\{\mathbf{F}_t, t = 1, \dots, T\}$.

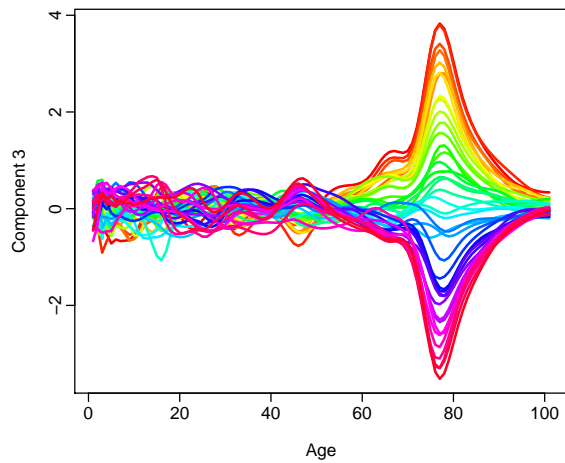
We use the Japanese sub-national mortality rates to evaluate the forecast accuracy. Using the expanding window analysis, we firstly use the first n observations to generate the h -step-ahead point forecasts for $h = 1, 2, \dots, T - n$. The forecast process is then iterated by increasing the sample size by one year until the data's end period. By doing so, we can produce one $(T - n)$ -step-ahead forecast, two $(T - n - 1)$ -step-ahead forecasts, \dots , and $(T - n)$ one-step-ahead forecasts. In this study, we use the data from 1975 to 2005 as the initial sample for forecasting, and then the sample increases by one year until 2015. We choose h being 10, so we obtain one 10-step-ahead forecast, two 9-step-ahead forecasts, \dots , and 10 one-step-ahead forecasts.



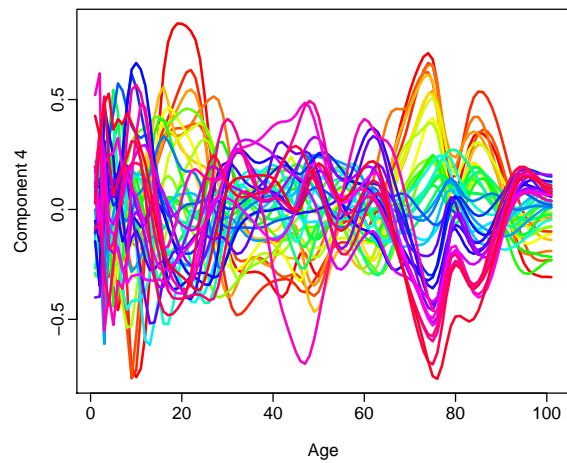
(a) First set of common functional time series



(b) Second set of common functional time series

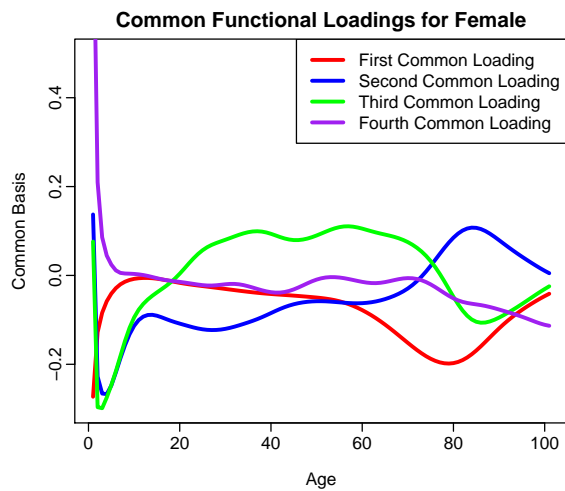


(c) Third set of common functional time series

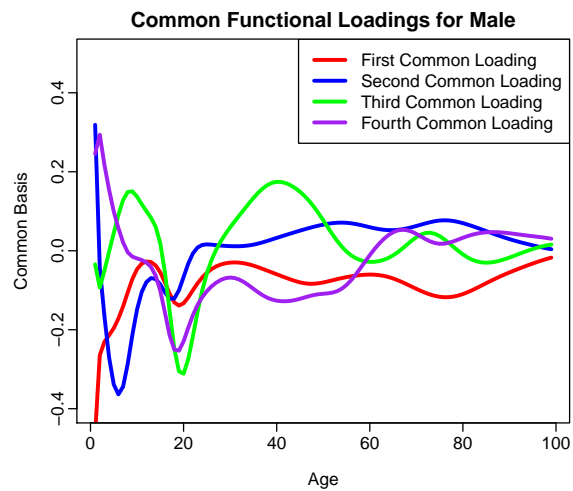


(d) Fourth set of common functional time series

Figure 3: First four sets of common functional time series of selected prefectures in Japan.



(a) Common factor loadings for female



(b) Common factor loadings for male

Figure 4: The first four common factor loadings for female and male

Table 3: The first six normalized eigenvalues for the auto-cross-covariance function of the common functional time series and the long-run-covariance function of four selected prefectures for both genders are reported. The eigenvalues for the auto-cross-covariance function of the common functional time series are labeled as “Common”, and the eigenvalues for the long-run-covariance function of the functional time series are labeled as “Specific”.

	Female					Male				
	Common	Specific				Common	Specific			
		Tokyo	Nagano	Kyoto	Osaka		Tokyo	Nagano	Kyoto	Osaka
1 st	0.901	0.973	0.957	0.961	0.971	0.873	0.959	0.933	0.937	0.956
2 nd	0.055	0.018	0.026	0.018	0.016	0.048	0.019	0.024	0.029	0.024
3 rd	0.023	0.004	0.007	0.010	0.006	0.032	0.012	0.015	0.013	0.008
4 th	0.008	0.002	0.004	0.005	0.004	0.021	0.004	0.009	0.008	0.005
5 th	0.007	0.001	0.002	0.003	0.002	0.009	0.002	0.005	0.005	0.003
6 th	0.003	0.001	0.001	0.002	0.001	0.006	0.001	0.005	0.003	0.002
Sum	0.997	0.999	0.997	0.999	1.000	0.989	0.997	0.991	0.995	0.998

We compare the proposed method with the high-dimensional functional time series (HDFTS, Gao et al., 2019), the high-dimensional functional factor model (HDFFM, Nisol et al., 2019), the factor models for matrix-valued high-dimensional time series (MFM, Wang et al., 2019) and the tensor decomposition forecast methods (Canonical Polyadic Decomposition (CPD) and Tucker) of Dong et al. (2020).

6.2.1 Point forecast accuracy

We use the root mean square forecast error (RMSFE) to evaluate the point forecast accuracy. The RMSFE measures how close the forecast results are to the actual values of the data under forecast. The RMSFE for the h -step-ahead forecasts of the i^{th} prefecture for $i \in \{1, \dots, 47\}$ can be written as

$$\text{RMSFE}^{(i)}(h) = \sqrt{\frac{1}{J \times (T - n - h + 1)} \sum_{\kappa=n}^{T-h} \sum_{j=1}^J [\mathcal{X}_{\kappa+h}^{(i)}(u_j) - \hat{\mathcal{X}}_{\kappa+h|\kappa}^{(i)}(u_j)]^2},$$

where κ is the number of observations used in generating the point forecasts, $\mathcal{X}_{\kappa+h}^{(i)}(u_j)$ is the actual value of the $(\kappa + h)^{\text{th}}$ curve of the i^{th} prefecture and $\hat{\mathcal{X}}_{\kappa+h}^{(i)}(u_j)$ is the h -step-ahead point forecast

based on the first κ observations, and J is the number of grid points on each curve. We use the average RMSFE for the h -step-ahead forecasts across all prefectures to reflect the accuracy of the h -step-ahead point forecasts:

$$\overline{\text{RMSFE}}(h) = \frac{1}{N} \sum_{i=1}^N \text{RMSFE}^{(i)}(h).$$

Table 4 tabulates the average RMSFE values across all prefectures for 1-step ahead to 10-step ahead forecast of different forecast methods. The bold entries highlight the method that produces the most accurate point forecast. Forecasts based on the proposed method have the smallest average RMSFE for both male and female mortality, which indicates that the proposed method outperforms other methods in terms of point forecast. This implies that the proposed model extracts the most information contained in the HDFTS.

Table 4: Average RMSE values ($\times 100$) in the holdout sample based on various forecasting methods are presented. Forecasts based on the proposed method are labeled as “FVP”, forecasts based on high dimensional functional time series are labeled as “HDFTS”, forecasts based on High dimensional functional factor models are labeled as “HDFFM”, forecasts based on matrix factor model are labeled as “MFM”, forecasts based on CPD tensor decompositions are labeled as “CPD” and forecasts based on Tucker tensor decompositions are labeled as “Tucker”.

Sex	h	FVP	HDFTS	HDFFM	MFM	CPD	Tucker
Female	1	0.896	2.294	2.801	2.339	1.522	1.631
	2	0.925	2.332	2.843	2.385	1.539	1.657
	3	0.995	2.360	2.872	2.301	1.535	1.656
	4	1.033	2.399	2.913	2.386	1.558	1.714
	5	1.013	2.400	2.911	2.552	1.554	1.651
	6	0.949	2.441	2.954	2.550	1.576	1.679
	7	0.873	2.515	3.037	2.383	1.624	1.670
	8	0.878	2.613	3.163	2.257	1.675	1.743
	9	0.881	2.735	3.302	2.176	1.775	1.861
	10	0.925	2.771	3.344	2.244	1.832	1.836
	Mean	0.937	2.486	3.014	2.357	1.619	1.710
	h	FVP	HDFTS	HDFFM	MFM	CPD	Tucker
Male	1	1.200	1.847	3.483	3.109	3.139	3.341
	2	1.206	1.872	3.259	2.997	3.176	3.401
	3	1.271	1.887	3.138	2.762	3.179	3.411
	4	1.270	1.922	2.945	2.649	3.207	3.460
	5	1.261	1.929	2.773	2.619	3.270	3.492
	6	1.295	1.979	2.593	2.788	3.373	3.615
	7	1.244	2.054	2.381	2.910	3.386	3.704

8	1.258	2.146	2.458	2.864	3.410	3.829
9	1.129	2.250	2.414	3.154	3.551	3.971
10	1.014	2.320	2.735	2.705	3.459	4.235
Mean	1.215	2.021	2.818	2.856	3.315	3.646

6.2.2 Interval forecast accuracy

We use the interval scoring rule of [Gneiting and Raftery \(2007\)](#) to evaluate the point-wise interval forecast accuracy. The interval score for the point-wise prediction interval of the i^{th} prefecture at time point u_j is

$$\begin{aligned}
S_\alpha \left[\widehat{\mathcal{X}}_{\kappa+h|\kappa}^{(i)\text{lb}}(u_j), \widehat{\mathcal{X}}_{\kappa+h|\kappa}^{(i)\text{ub}}(u_j); \mathcal{X}_{\kappa+h}^{(i)}(u_j) \right] &= \left[\widehat{\mathcal{X}}_{\kappa+h|\kappa}^{(i)\text{ub}}(u_j) - \widehat{\mathcal{X}}_{\kappa+h|\kappa}^{(i)\text{lb}}(u_j) \right] \\
&+ \frac{2}{\alpha} \left[\widehat{\mathcal{X}}_{\kappa+h|\kappa}^{(i)\text{lb}}(u_j) - \mathcal{X}_{\kappa+h}^{(i)}(u_j) \right] \mathbb{1} \left\{ \mathcal{X}_{\kappa+h}^{(i)}(u_j) < \widehat{\mathcal{X}}_{\kappa+h|\kappa}^{(i)\text{lb}}(u_j) \right\} \\
&+ \frac{2}{\alpha} \left[\mathcal{X}_{\kappa+h}^{(i)}(u_j) - \widehat{\mathcal{X}}_{\kappa+h|\kappa}^{(i)\text{ub}}(u_j) \right] \mathbb{1} \left\{ \mathcal{X}_{\kappa+h}^{(i)}(u_j) > \widehat{\mathcal{X}}_{\kappa+h|\kappa}^{(i)\text{ub}}(u_j) \right\},
\end{aligned}$$

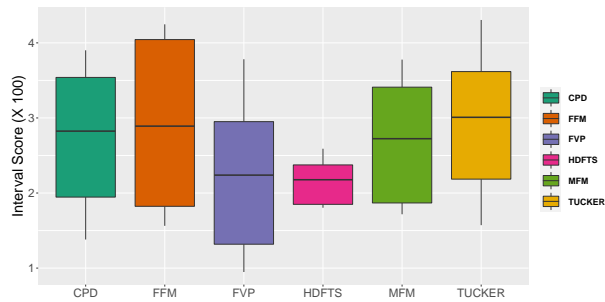
where the level of significance α can be chosen conventionally as 0.2. It is not difficult to find that the smaller the interval score, the more accurate the interval forecast. An optimal (which is also minimal) interval score value can be achieved if $\mathcal{X}_{\kappa+h}^{(i)}(u_j)$ lies between $\widehat{\mathcal{X}}_{\kappa+h|\kappa}^{(i)\text{lb}}(u_j)$ and $\widehat{\mathcal{X}}_{\kappa+h|\kappa}^{(i)\text{ub}}(u_j)$. Then the mean interval score for the h -step-ahead forecasts of the i^{th} prefecture can be written as

$$\overline{S}_\alpha^{(i)}(h) = \frac{1}{J \times (T - n - h + 1)} \sum_{\kappa=n}^{T-h} \sum_{j=1}^J S_\alpha \left[\widehat{\mathcal{X}}_{\kappa+h|\kappa}^{(i)\text{lb}}(u_j), \widehat{\mathcal{X}}_{\kappa+h|\kappa}^{(i)\text{ub}}(u_j); \mathcal{X}_{\kappa+h}^{(i)}(u_j) \right].$$

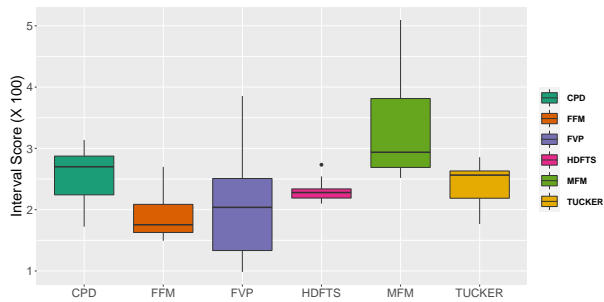
We use the average mean interval score for the h -step-ahead forecasts across all prefectures to reflect the accuracy of the h -step-ahead point-wise prediction interval:

$$\overline{S}_\alpha(h) = \frac{1}{N} \sum_{i=1}^N \overline{S}_\alpha^{(i)}(h).$$

Figure 5 shows the side-by-side box plots of average mean interval score values across all prefectures for one-step ahead to 10-step ahead forecast of different forecast methods. From the box plots, despite HDFTS performs better for female mortality while FFM performs better for male mortality, the proposed method could generate relatively smaller average mean interval score values for some of the forecast horizons, which demonstrates that the proposed method could produce more accurate interval forecasts.



(a) Interval scores of various methods for female mortality



(b) Interval scores of various methods for male mortality

Figure 5: Average interval score values ($\times 100$) in the holdout sample of various forecasting methods.

After comparing the point and interval forecast results of various methods, our proposed method outperforms other competitive methods in forecasting the HDFTS. This indicates that the dimension reduction of the proposed model is efficient in capturing both the serial dependence and the correlation among cross-sections in the high-dimensional time series.

6.3 Life annuity Pricing

Life annuities have been one of the typical longevity insurance products for people to finance their retirements. Rapid improvements in mortality have exposed life insurers with longevity risk (Ngai and Sherris, 2011). Accurate mortality forecasts could enable life insurers to manage longevity risk effectively without holding excessive levels of capital. To illustrate the impact of the forecasting improvements, we use the mortality forecasts to price the life annuities, i.e., the amount of money an individual pays for life insurer in return for annual payments after retirement until death. We compare the present values of the life annuities based on mortality forecasts from different methods. The present values of the life annuities represent how much capital that the life insurer should reserve.

In the life annuity comparison, we calculate the present value of the life annuity with \$1 annual payments. More specifically, the price of a life annuity for an individual aged x at year t is the present value of the annual payments of \$1 that the individual receives after retirement until death or a pre-agreed age (which one occurs first). The retirement age is set to be 65, and the pre-agreed age that the annuity terminates is assumed to be 90 (He et al., 2021). Then the price of the annuity

can be calculated as:

$$PV_{x,t} = \begin{cases} \sum_{n=1}^{90-x} \frac{{}_n p_{x,t}}{(1+i)^n}, & x \geq 65 \\ \sum_{n=1}^{25} \frac{{}_n p_{65,t+(65-x)}}{(1+i)^{n+(65-x)}}, & x < 65, \end{cases}$$

where $PV_{x,t}$ is the present value of the life annuity for an individual aged x at year t , ${}_n p_{x,t}$ is the survival probability for an individual aged x at year t to survive after n years, and i is the interest rate used for discounting. For an individual older than 65-year-old, they receive payment for each year of survival, and for an individual younger than 65-year-old, the annuity is deferred with the first payment paid out at the year that they survive their 66th birthday.

To demonstrate the financial impact of the forecasting improvement in mortality, we compare the annuity prices based on mortality forecast using different methods. We use the Japanese sub-national mortality data of 47 prefectures from 1975 to 2005 as training dataset and the data from the years 2006 to 2015 as testing data. We forecast the mortality rates for the testing data based on the training data using different methods. Then we calculate the annuity prices, $PV_{x,t}$ using the forecasts of mortality rates from different methods as well as the actual mortality rates.

Table 5: Average annuity prices with annual payment \$1 and interest rate 2% for selected ages and years. Annuity prices based on true mortality rates are labeled as "TRUE", annuity prices based on the proposed method are labeled as "FVP", annuity prices based on high dimensional functional time series are labeled as "HDFTS", annuity prices based on High dimensional functional factor models are labeled as "HDFFM", annuity prices based on matrix factor model are labeled as "MFM", annuity prices based on CPD tensor decompositions are labeled as "CPD" and annuity prices based on Tucker tensor decompositions are labeled as "Tucker".

Sex	(Year, Age)	TRUE	FVP	HDFTS	HDFFM	MFM	CPD	Tucker
Female	1980, 55	13.030	13.074	12.605	12.530	12.758	12.901	12.956
	1985, 60	14.728	14.778	14.248	14.163	14.421	14.582	14.645
	1990, 65	15.791	15.848	15.244	15.147	15.440	15.625	15.696
	1995, 70	12.986	13.052	12.351	12.239	12.579	12.793	12.876
	2000, 75	10.049	10.128	9.296	9.161	9.565	9.820	9.918
	2005, 80	6.983	7.082	6.049	5.881	6.383	6.699	6.821
	2010, 85	3.780	3.883	3.347	3.250	3.490	3.636	3.697
	(Year, Age)	TRUE	FVP	HDFTS	HDFFM	MFM	CPD	Tucker
Male	1980, 55	10.084	10.119	9.871	9.836	9.915	10.035	10.127
	1985, 60	11.702	11.742	11.454	11.414	11.506	11.644	11.751
	1990, 65	12.867	12.916	12.575	12.526	12.635	12.800	12.926
	1995, 70	10.417	10.476	10.055	9.995	10.130	10.333	10.489

2000, 75	7.988	8.066	7.518	7.439	7.614	7.880	8.082
2005, 80	5.580	5.692	4.907	4.792	5.044	5.424	5.715
2010, 85	3.167	3.279	2.845	2.780	2.904	3.084	3.216

Table 5 exhibits the average prices of annuities with annual payment \$1 and interest rate 2% for some selected ages and years. It is clear to see that most of the forecasting methods tend to underestimate the annuity prices, which is a common phenomenon in actuarial studies, which corresponds to the underestimated longevity risk (Ngai and Sherris, 2011). However, our methods slightly overestimate the annuity prices. Further investigation of the annuity prices reveals that the pricing errors of the proposed method are much lower than those of other methods.

To illustrate the financial impact of the mispricing on life insurers, consider the annuity pricing for females aged 75 at year 2000. The pricing error for the proposed method is \$0.079 per \$1 payment. However, the pricing errors for other competing methods range from \$0.131 to \$0.888 per \$1 payment. Suppose the annual payment for each individual is \$10,000, and 50,000 people purchased this product. Then based on the proposed method, the capital that the insurer needs to reserve is reduced by at least 26 million $\left((\$0.131 - \$0.079) \times 10,000 \times 50,000 = \$26\text{million} \right)$, which is a significant saving to the life insurer.

7 Conclusion

In this paper, we propose a factor model for HDFTS. By separating the heterogeneity out, we can reduce the HDFTS into a functional time series of low dimensions. Then a common functional front loading can be determined such that the temporal information in HDFTS can be extracted into a low-dimensional functional time series. The proposed model provides us more flexibility, with some certain choices of the front and back loadings; our model coincides with some of the existing factor models for HDFTS.

Through a Monte Carlo simulation, we demonstrate the performance of the proposed method in model fitting. An empirical study on the age-specific mortality rates of 47 Japanese prefectures demonstrates the superiority of the proposed method over the existing models in terms of forecasting, showing that the proposed model can extract the temporal information more effectively.

The proposed model can be viewed as a functional panel data model with interactive effects. We considered the multiplicity of time trend effects and country-specific effects instead of the

addition as in the additive fixed effects models.

One possible future study would be to extend the functional concurrent regression in the proposed model to the functional time series regression of [Pham and Panaretos \(2018\)](#). Since in the current work, functional concurrent regression is performed for each $t \in \{1, \dots, T\}$ to obtain the functional time series of lower dimension, which ignores the temporal dependence of the functional observations. This awaits further investigation.

References

- Andrews, D. (1991), 'Heteroskedasticity and autocorrelation consistent covariant matrix estimation', *Econometrica* **59**(3), 817–858.
- Bai, J. (2009), 'Panel data models with interactive fixed effects', *Econometrica* **77**(4), 1229–1279.
- Bathia, N., Yao, Q., Ziegelmann, F. et al. (2010), 'Identifying the finite dimensionality of curve time series', *The Annals of Statistics* **38**(6), 3352–3386.
- Bellman, R. (1966), 'Dynamic programming', *Science* **153**(3731), 34–37.
- Bühlmann, P. and Van De Geer, S. (2011), *Statistics for High-dimensional Data: Methods, Theory and Applications*, Springer Science & Business Media, Berlin.
- Cai, T. and Chen, X. (2010), *High-dimensional Data Analysis*, Higher Education Press, Beijing.
- Chang, J., Chen, C. and Qiao, X. (2020), 'An autocovariance-based learning framework for high-dimensional functional time series', *arXiv preprint arXiv:2008.12885* .
URL: <https://arxiv.org/abs/2008.12885>
- Chiou, J.-M. (2012), 'Dynamical functional prediction and classification, with application to traffic flow prediction', *The Annals of Applied Statistics* **6**(4), 1588–1614.
- Di, C.-Z., Crainiceanu, C. M., Caffo, B. S. and Punjabi, N. M. (2009), 'Multilevel functional principal component analysis', *The Annals of Applied Statistics* **3**(1), 458–488.
- Dong, Y., Huang, F., Yu, H. and Haberman, S. (2020), 'Multi-population mortality forecasting using tensor decomposition', *Scandinavian Actuarial Journal* pp. 1–22.
- Ferraty, F. and Vieu, P. (2006), *Nonparametric Functional Data Analysis: Theory and Practice*, Springer Science & Business Media, Berlin.
- Freyberger, J. (2018), 'Non-parametric panel data models with interactive fixed effects', *The Review of Economic Studies* **85**(3), 1824–1851.
- Gallant, A. R. (2009), *Nonlinear Statistical Models*, John Wiley & Sons, Hoboken, New Jersey.
- Gao, Y., Shang, H. L. and Yang, Y. (2019), 'High-dimensional functional time series forecasting: An application to age-specific mortality rates', *Journal of Multivariate Analysis* **170**, 232 – 243.

- Gaskin, C. J. and Happell, B. (2014), 'On exploratory factor analysis: A review of recent evidence, an assessment of current practice, and recommendations for future use', *International Journal of Nursing Studies* **51**(3), 511–521.
- Giroso, F. and King, G. (2008), *Demographic forecasting*, Princeton University Press, Princeton, New Jersey.
- Gneiting, T. and Raftery, A. E. (2007), 'Strictly proper scoring rules, prediction, and estimation', *Journal of the American statistical Association: Review Article* **102**(477), 359–378.
- Hall, P. and Vial, C. (2006), 'Assessing the finite dimensionality of functional data', *Journal of the Royal Statistical Society: Series B (Statistical Methodology)* **68**(4), 689–705.
- Hansen, L. P. (1982), 'Large sample properties of generalized method of moments estimators', *Econometrica: Journal of the Econometric Society* **50**(4), 1029–1054.
- Hays, S., Shen, H., Huang, J. Z. et al. (2012), 'Functional dynamic factor models with application to yield curve forecasting', *The Annals of Applied Statistics* **6**(3), 870–894.
- He, L., Huang, F. and Yang, Y. (2021), 'Data-adaptive dimension reduction for us mortality forecasting', *arXiv preprint arXiv:2102.04123* .
URL: <https://arxiv.org/abs/2102.04123>
- Hörmann, S. and Kidziński, Ł. (2015), 'A note on estimation in Hilbertian linear models', *Scandinavian Journal of Statistics* **42**(1), 43–62.
- Hörmann, S., Kidziński, Ł. and Hallin, M. (2015), 'Dynamic functional principal components', *Journal of the Royal Statistical Society: Series B (Statistical Methodology)* **77**(2), 319–348.
- Hörmann, S., Kokoszka, P. et al. (2010), 'Weakly dependent functional data', *The Annals of Statistics* **38**(3), 1845–1884.
- Horváth, L. and Kokoszka, P. (2012), *Inference For Functional Data with Applications*, Springer Science & Business Media, New York.
- Horváth, L., Kokoszka, P. and Reeder, R. (2013), 'Estimation of the mean of functional time series and a two-sample problem', *Journal of the Royal Statistical Society: Series B (Statistical Methodology)* **75**(1), 103–122.

- Hyndman, R. J. and Shang, H. L. (2010), 'Rainbow plots, bagplots, and boxplots for functional data', *Journal of Computational and Graphical Statistics* **19**(1), 29–45.
- Hyndman, R. J. and Ullah, M. S. (2007), 'Robust forecasting of mortality and fertility rates: A functional data approach', *Computational Statistics & Data Analysis* **51**(10), 4942–4956.
- Japan Mortality Database (2021), *National Institute of Population and Social Security Research*.
URL: <http://www.ipss.go.jp/p-toukei/JMD/>
- Jolliffe, I. T. and Cadima, J. (2016), 'Principal component analysis: a review and recent developments', *Philosophical Transactions of the Royal Society A: Mathematical, Physical and Engineering Sciences* **374**(2065), 20150202.
- Jungbacker, B., Koopman, S. J. and Van Der Wel, M. (2014), 'Smooth dynamic factor analysis with application to the US term structure of interest rates', *Journal of Applied Econometrics* **29**(1), 65–90.
- Kokoszka, P., Miao, H. and Zhang, X. (2015), 'Functional dynamic factor model for intraday price curves', *Journal of Financial Econometrics* **13**(2), 456–477.
- Kokoszka, P. and Reimherr, M. (2017), *Introduction to Functional Data Analysis*, CRC press, Cleveland.
- Lam, C., Yao, Q. and Bathia, N. (2011), 'Estimation of latent factors for high-dimensional time series', *Biometrika* **98**(4), 901–918.
- Lam, C., Yao, Q. et al. (2012), 'Factor modeling for high-dimensional time series: Inference for the number of factors', *The Annals of Statistics* **40**(2), 694–726.
- Lee, R. D. and Carter, L. R. (1992), 'Modeling and forecasting US mortality', *Journal of the American Statistical Association: Application & Case Studies* **87**(419), 659–671.
- Li, J. (2013), 'A Poisson common factor model for projecting mortality and life expectancy jointly for females and males', *Population Studies* **67**(1), 111–126.
- Li, N. and Lee, R. (2005), 'Coherent mortality forecasts for a group of populations: An extension of the lee-carter method', *Demography* **42**(3), 575–594.
- Li, N., Lee, R. and Gerland, P. (2013), 'Extending the Lee-Carter method to model the rotation of age patterns of mortality decline for long-term projections', *Demography* **50**(6), 2037–2051.

- Liebl, D. et al. (2013), 'Modeling and forecasting electricity spot prices: A functional data perspective', *The Annals of Applied Statistics* **7**(3), 1562–1592.
- Martínez-Hernández, I., Gonzalo, J. and González-Farías, G. (2020), 'Nonparametric estimation of functional dynamic factor model', *arXiv preprint arXiv:2011.01831* .
URL: <https://arxiv.org/abs/2011.01831>
- Newey, W. K. and West, K. D. (1987), 'A simple, positive semi-definite, heteroskedasticity and autocorrelation consistent covariance matrix', *Econometrica* **55**(3), 703–708.
- Ngai, A. and Sherris, M. (2011), 'Longevity risk management for life and variable annuities: The effectiveness of static hedging using longevity bonds and derivatives', *Insurance: Mathematics and Economics* **49**(1), 100–114.
- Nisol, G., Tavakoli, S. and Hallin, M. (2019), 'High-dimensional functional factor models', *arXiv preprint arXiv:1905.10325* .
URL: <https://arxiv.org/abs/1905.10325>
- Pampel, F. (2005), 'Forecasting sex differences in mortality in high income nations: The contribution of smoking', *Demographic Research* **13**(18), 455–484.
- Panaretos, V. M. and Tavakoli, S. (2013a), 'Cramér–Karhunen–Loève representation and harmonic principal component analysis of functional time series', *Stochastic Processes and their Applications* **123**(7), 2779–2807.
- Panaretos, V. M. and Tavakoli, S. (2013b), 'Fourier analysis of stationary time series in function space', *The Annals of Statistics* **41**(2), 568–603.
- Pham, T. and Panaretos, V. M. (2018), 'Methodology and convergence rates for functional time series regression', *Statistica Sinica* **28**(4), 2521–2539.
- Politis, D. N. and Romano, J. P. (1996), 'On flat-top kernel spectral density estimators for homogeneous random fields', *Journal of Statistical Planning and Inference* **51**(1), 41–53.
- Politis, D. N. and Romano, J. P. (1999), 'Multivariate density estimation with general flat-top kernels of infinite order', *Journal of Multivariate Analysis* **68**(1), 1–25.

- Ramsay, J. O., Hooker, G. and Graves, S. (2009), *Functional Data Analysis with R and MATLAB*, Springer, New York.
- Ramsay, J. O. and Silverman, B. W. (2006), *Functional Data Analysis*, Springer Science & Business Media, New York.
- Renshaw, A. E. and Haberman, S. (2003), 'Lee–carter mortality forecasting with age-specific enhancement', *Insurance: Mathematics and Economics* **33**(2), 255–272.
- Rice, G. and Shang, H. L. (2017), 'A plug-in bandwidth selection procedure for long-run covariance estimation with stationary functional time series', *Journal of Time Series Analysis* **38**(4), 591–609.
- Rice, J. A. and Silverman, B. W. (1991), 'Estimating the mean and covariance structure nonparametrically when the data are curves', *Journal of the Royal Statistical Society. Series B (Statistical Methodology)* **53**(1), 233–243.
- Shang, H. L. (2016), 'Mortality and life expectancy forecasting for a group of populations in developed countries: a multilevel functional data method', *The Annals of Applied Statistics* **10**(3), 1639–1672.
- Shang, H. L. (2018), 'Bootstrap methods for stationary functional time series', *Statistics and Computing* **28**(1), 1–10.
- Tang, C., Shang, H. L. and Yang, Y. (2021), 'Clustering and forecasting multiple functional time series', *The Annals of Applied Statistics*, revised and resubmitted .
- Tsay, R. S. (2013), *Multivariate Time Series Analysis: with R and Financial Applications*, John Wiley & Sons, New York.
- Wang, D., Liu, X. and Chen, R. (2019), 'Factor models for matrix-valued high-dimensional time series', *Journal of Econometrics* **208**(1), 231–248.
- White, H. (1984), *Asymptotic Theory for Econometricians*, Academic press, Cambridge, Massachusetts.
- Wiśniowski, A., Smith, P. W., Bijak, J., Raymer, J. and Forster, J. J. (2015), 'Bayesian population forecasting: Extending the lee-carter method', *Demography* **52**(3), 1035–1059.
- Yao, F., Müller, H.-G. and Wang, J.-L. (2005), 'Functional data analysis for sparse longitudinal data', *Journal of the American Statistical Association: Theory and Methods* **100**(470), 577–590.